Geophys. J. Int. (2010) **181,** 502–520 doi: 10.1111/j.1365-246X.2010.04516.x

Love-wave group velocity maps of Turkey and surrounding regions

M. Didem Cambaz and Hayrullah Karabulut

Bogazici University, Kandilli Observatory and Earthquake Research Institute, 36684, *Cengelkoy Istanbul, Turkey. E-mail: kara@boun.edu.tr*

Accepted 2010 January 8. Received 2009 December 23; in original form 2009 February 15

SUMMARY

We present the analysis of a Love-wave dispersion study performed across Turkey and the surroundings. Group velocity dispersion curves were obtained from the local and regional earthquakes recorded at both permanent and temporary stations operated in the region. Love-wave group velocity maps in the period range of 10–50 s were computed using a tomographic inversion method. The study shows the existence of significantly different crustal types in the area. The group velocity anomalies are associated with the major geological structures in the region. Low group velocities at shorter periods (10–20 s) are observed in the local sedimentary basins, the eastern Mediterranean and the Black Sea. The eastern Anatolia region is also characterized by low group velocities while Pontides and Bitlis–Pötürge massif display higher group velocities. The central Anatolia exhibits uniform velocity distribution indicating more homogenous crust. The Isparta angle is marked by a wedge-shaped low group velocity anomaly. The low velocities observed in the Isparta angle are related to crustal thickening and subduction-related complex. High velocities observed on the maps are associated with metamorphics, magmatic arcs along the orogenic belts of Pontides, Pötürge massif and crustal thinning in the Aegean region. At larger periods (40–50 s) the Anatolian block shows low and uniform group velocity distribution while its surroundings display higher group velocities with the exception of the eastern Mediterranean region.

Key words: Composition of the continental crust; Surface waves and free oscillations; Seismic tomography.

1 INTRODUCTION

Surface wave tomography has proven to be very useful in determining the structure of the crust and uppermost mantle on both regional and global scale (Dziewonski 1971; Woodhouse & Dziewonski 1984; Trampert & Woodhouse 1995; van Heijst & Woodhouse 1999). Their large amplitudes with relatively low attenuation and long propagation paths have provided significant contribution to our knowledge of the Earth's upper-mantle and crustal structure. One-dimensional earth models have been routinely obtained along great circle paths using the dispersive nature of surface waves (Oliver 1962; Knopoff 1972) while long-period surface waves have been the main source of the observation for determining the tomographic image of the mantle.

During the last decade with the availability of high-quality digital broad-band seismic data we have seen a rapid progress in imaging the structure of crust and upper mantle with increasing resolutions. Studies at local and regional scales are now common for regions with a good coverage of stations and earthquakes. Phase- and group-velocity distributions obtained from dispersive surface waves correlate well with the main tectonic belts and geological units providing better constrains on their geometry and relation to the regional tectonics (Levshin *et al.* 1992, 1994; Ritzwoller *et al.* 2002; Pasyanos 2005).

Turkey and the surrounding areas have been the target of many geophysical studies due to its active tectonics and high seismicity rate. Continuous regional deformation along the seismically active boundaries contains diverse structures such as suture zones, metamorphic core complexes and young orogens (Stampfli 2000 and references therein). Significant variations exist on the tectonic styles and crustal structures. Until recently, investigations on the crustal thickness and seismic velocities used sparse distribution of seismic stations in the region (e.g. Mindevalli & Mitchell 1989; Saunders *et al.* 1998; Maggi & Priestly 2005). Temporary experiments along with the existing data from the permanent seismic stations provided more details on the lithospheric structure and composition (e.g. Al-Lazki *et al.* 2003; Gök *et al.* 2003; Sandvol *et al.* 2003; Zor *et al.* 2003; Zhu *et al.* 2006). Some other works have also been performed in the region at greater scales to estimate group- and phase-velocity variations (e.g. Curtis *et al.* 1998; Ritzwoller & Levshin 1998; Pasyanos *et al.* 2001; Karagianni *et al.* 2002, 2005; Pasyanos 2005; Sodoudi *et al.* 2006; DiLuccio & Pasyanos 2007; Gök *et al.* 2007).

In this study, we obtained Love-wave group velocity maps for 10–50 s periods using local and regional earthquakes. We used available data from the broad-band stations operated between 1997 and 2009 in Turkey and the surrounding regions. We analysed 285 earthquakes with magnitudes greater than 4.5. Fundamental mode group

© 2010 The Authors
Journal compilation © 2010 RAS

velocities of Love and Rayleigh waves at more than 270 broad-band stations along 13 171 paths were computed using Multiple-filter analysis (MFA; Dziewonski *et al.* 1969; Pedersen *et al.* 2003). Approximately 25 per cent of the paths for Love waves provided reliable group velocity measurements. The group velocity maps were interpreted in relation to the geological and tectonic observations in the region.

2 TECTONICS AND GEOLOGY

Turkey is an east–west trending segment of the Alpine–Himalayan orogenic belt and located on the boundary between Gondwana in the south and Laurasia in the north. Within this belt different continental and oceanic assemblages related to the opening and closure of the Paleozoic and Mesozoic oceanic basins can be found. These basins are collectively named the Tethys Ocean (Göncüoğlu *et al.* 1997). Although the geometry and evolution of the Tethys Ocean is still in debate, there is a consensus regarding the presence of Paleotethys on the north and Neotethys on the south both rifted from the Gondwana margin (Stampfli 2000). The present tectonic regime of Turkey follows closure and the destruction of the Neo-Tethyan oceans (Fig. 1).

The northern Neotethys is located between the Sakarya continent in the north and the Anatolian–Tauride Platform in the south. The southern Neotethys, which separated Arabian Platform in the south from Anatolide–Tauride Platform in the north, is located along the Southeast Anatolian Suture. Two major E–W trending ophiolite belts indicate the closure and destruction of Neotethys (Stampfli 2000).

Various continental blocks that make up present-day tectonics of Turkey are mainly divided into six major lithospheric fragments; the Strandja, the Istanbul (IZ) and the Sakarya zones (SZ), the Antolide–Tauride Block (A–T), the Kirşehir Massif (KM) and the Arabian Platform (Şengör & Yılmaz 1981; Şengör *et al.* 1982; Okay 1989; Okay *et al.* 1994).

The Strandja, Istanbul and Sakarya zones show similar geological patterns with Laurasia and are referred as the Pontides. The İzmir–Ankara–Erzincan suture separates these units with the KM and the A–T block which show similar Paleozoic stratigraphy with the Arabian Platform as well as northern margin of Gondwana (Okay & Tüysüz 1999).

The IZ is characterized by a thick Ordovician to Carboniferous sedimentary sequence, which rests unconformably on a Precambrian metamorphic basement. It is bordered by the Strandja massif in the west, separated along the Intra-Pontide suture from the SZ in the south. The east–west oriented Intra-Pontide suture, marked by slivers of serpentinite, blueschist, basic volcanic rocks and pelagic limestone is the remnant of the Mesozoic Intra-Pontide ocean (Şengör & Yılmaz 1981).

The A–T block forms the main part of the southern Turkey. This unit has a Paleozoic stratigraphy similar to the Arabian platform and Gondwana. There is a massive ophiolite and accretionary complex accumulation over this block. The A–T block can be described in three regional metamorphic complexes: the Tavşanlı zone, the Afyon zone and the Menderes Massif. The Bornova Flysch Zone in this block exists between the İzmir–Ankara–Erzincan suture and the Menderes Massif (Okay & Tüysüz 1999).

The central Anatolia displays a transitional character between the extensional tectonic regime of the western Anatolia and the

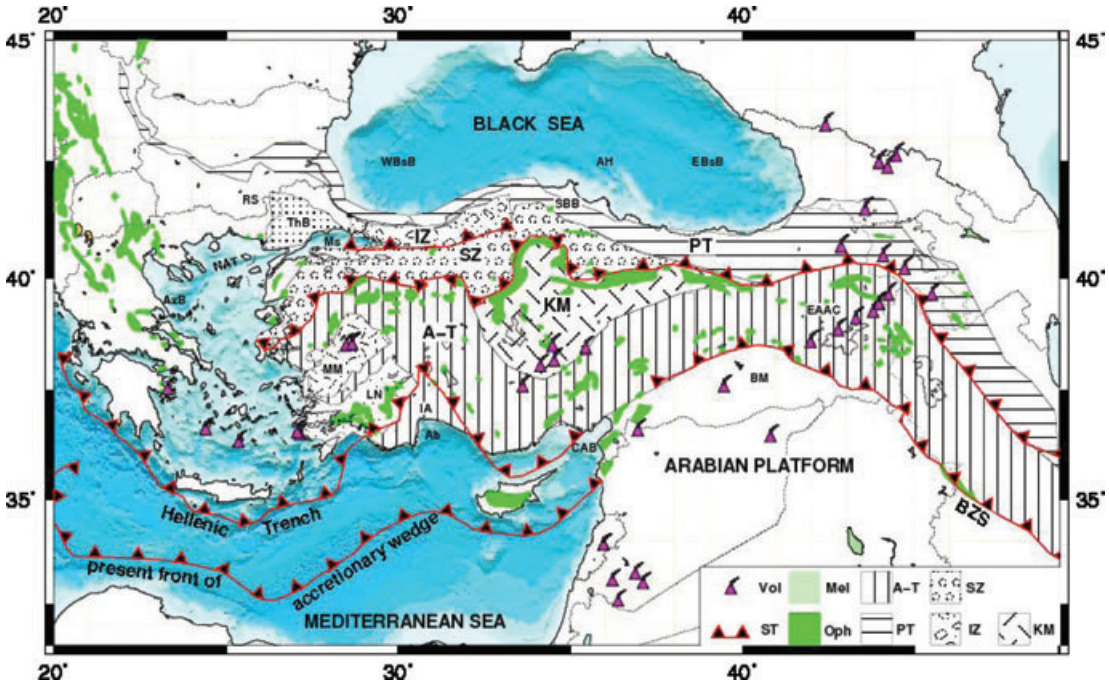

Figure 1. Tectonic setting of Turkey and surrounding areas; Abbreviations: AH, Andrusov High; AxB, Axion Basin; A–T, Anatolid–Tauride Block; BM, Bitlis Massif; BZM, Bitlis–Zagros Suture; CAB, Ceyhan–Adana Basin; EBsB, Eastern Black Sea Basin; EAAC, East Anatolian Accretionary Complex; IA, Isparta Angle; IZ, Istanbul Zone; KM, Kırşehir Massif; LN, Lycian Nappes; Ms, Marmara Sea; MM, Menderes Massif; NAT, North Anatolian Through; PT, Pontides; RS, Rhodope–Strandja Zone; SBB, Sinop–Boyabat Basin; SZ, Sakarya Zone; ThB, Thrace Basin; WBsB, Western Black Sea Basin; Green units represent the ophiolites. Bathymetry of the region derived from ETOPO5. Purple volcano signs show Neogene and quaternary volcanism. Red triangles show the sutures and earlier subduction zones. (Modified from Stampfli, http://www-sst.unil.ch/research/plate tecto /present_day.htm; Okay & Tüysüz 1999; Robertson 2000; Tatar *et al.* 2000).

© 2010 The Authors, *GJI*, **181,** 502–520
Journal compilation © 2010 RAS

strike-slip tectonic regime of the eastern Anatolia. Most of the geological structures of the central Anatolia and the Taurides, including Isparta angle (IA), have been sourced from the tectonic and magmatic events related to the active convergent plate boundary, north-dipping Hellenic–Cyprus subduction zone (Glover & Robertson 1998).

In the central Anatolia, the KM consists of metamorphic and voluminous granitic rocks. These metamorphic rocks from Cretaceous age constitute a coherent metasedimentary sequence of granulite, gneiss, micashist, metaquarzite, marble and calc-silicate rocks. They are folded and multiply deformed (Seymen 1984; Okay & Tüysüz 1999). The accretionary complex and the metamorphic rocks, which are intruded by granitic rocks, cover large areas in the KM. The most prominent geological feature of the region is the widespread volcanism. The origin of the volcanism is considered to be arc related from the north-dipping oceanic slab of African Plate (Innocenti *et al.* 1982). However, more recent works also suggest that it can be related to regional extension (Toprak & Göncüoğlu 1993).

The Arabian Platform consists of marine, sedimentary succession accumulated from early Cambrian to middle Miocene time. Along the suture zone the ophiolits of the Arabian platform forms a giant nappe accumulation (Yılmaz 1993). The Bitlis Massif (BM) forming an E–W trending mountain range in southeast Anatolia is a metamorphic complex. Two tectonic units; an old, high-grade metamorphic core and a metamorphic cover representing a platform sequence constitute this massif (Yılmaz 1993). BM and its ophiolitic cover are fragmented by the rifting of the Maden Basin (MB). For this reason, the various ophiolit fragments were transported into the basin. Widespread volcanic activity accompanied the sedimentation in this region (Yılmaz 1993).

The Black Sea is composed of two deep basins (Fig. 2); the western Black Sea basin, which is underlain by oceanic to suboceanic crust, contains a sedimentary cover of up to 19 km thick. The eastern Black Sea basin, which is underlain by thinned continental crust, has 12 km thickness of sediments (Nikishin *et al.* 2003). These basins are separated by the Andrusov Ridge that is formed from continental crust and overlain by 5–6 km thickness of sedimentary cover (Robinson 1997).

3 DATA

A waveform database for the surface wave investigations was formed from the permanent and temporary digital broad-band stations in the region between 1997 and 2009 (Fig. 3). The main source of the data is the National Network of Turkey operated by Kandilli Observatory and Earthquake Research Institute. The network has been continuously upgraded since 2004 and the number of broad-band stations has exceeded 100 in 2008. The majority of the stations record at periods 100 s or higher. However, approximately 10 per cent of the instruments have lower recording range (<40 s). Supplementary data from IRIS and ORFEUS depository were obtained for the permanent stations in the region.

Data from several portable deployments were also included in the study. A temporary network with 29 broad-band stations operated between 1999 and 2001 during the Eastern Turkey Seismic Experiment (Sandvol *et al.* 2003). Data from local networks, which have been operating in the various regions of Turkey, also contributed to the database. As a result, the total number of stations exceeds 270 and distributed non-uniformly throughout the region. The station coverage is dense in the Marmara region and the eastern Anatolia while the central Anatolia, Black Sea and Eastern Mediterranean regions are poorly sampled.

We selected 285 earthquakes that occurred between 1997 and 2009 with magnitudes greater than 4.5 and depths less than 30 km (Fig. 3). The event distribution is also non-uniform. The majority

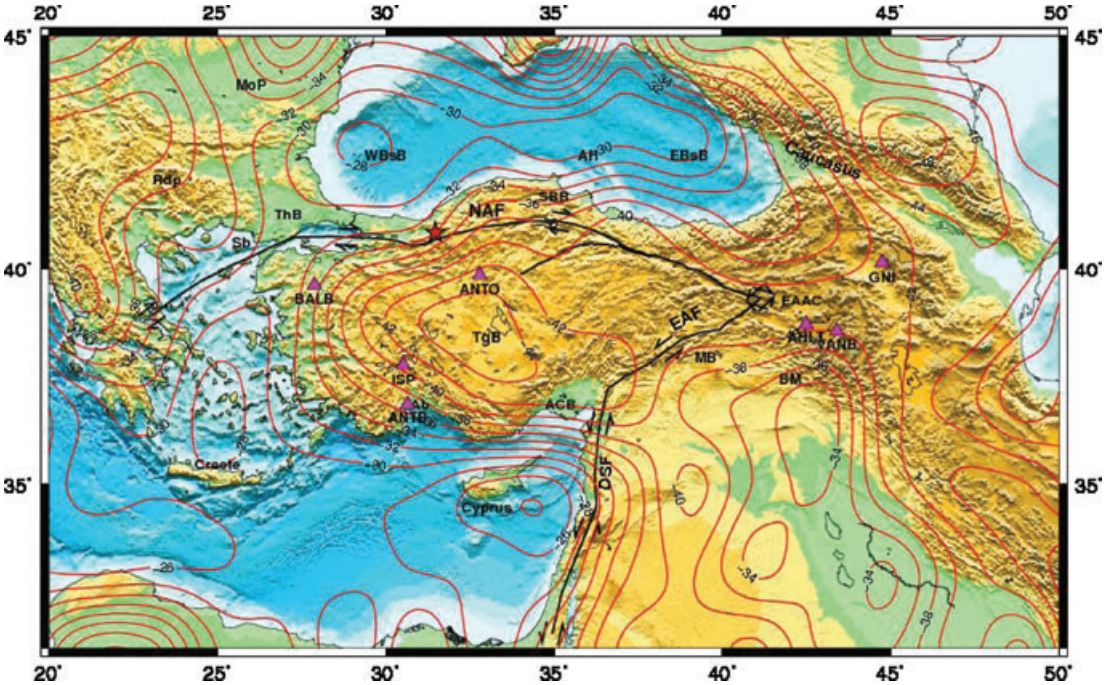

Figure 2. Topography, major fault lines and crustal thickness of Turkey and surrounding areas (Mooney *et al.* 1998); Abbreviations: EAF, East Anatolian Fault; MoP, Moesian Platform; NAF, North Anatolian Fault; TgB, Tuz Golu Basin; Sb, Saros Bay. The red star shows the location of an aftershock of November 12 Düzce earthquake ($M_w = 5.0$). The red triangles indicate the locations of the broad-band stations used for the construction dispersion curves in Fig. 12 from the group velocity maps. Bathymetry and Topography of the region derived from ETOPO5 and GTOPO30.

© 2010 The Authors, *GJI*, **181,** 502–520
Journal compilation © 2010 RAS

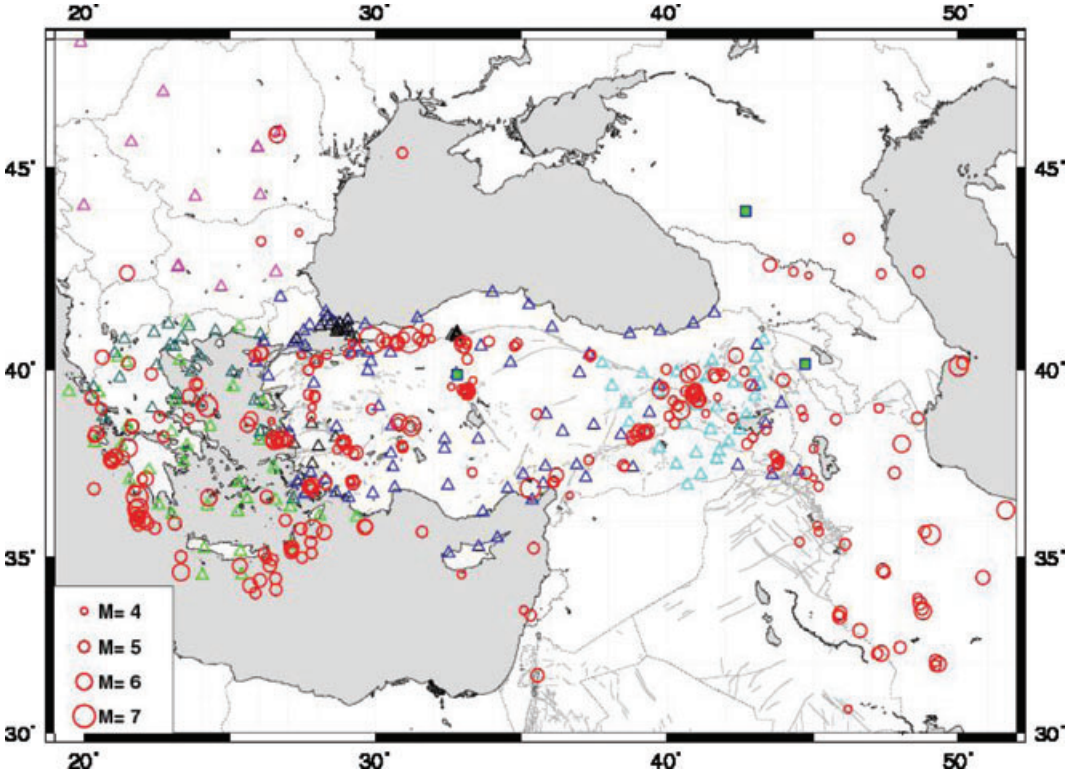

Figure 3. Distribution of earthquakes (circles) and seismic stations (triangles). The different colours indicate the stations from various networks (dark blue: KOERI; light green: NOA; dark green: THE; light blue: ETSE; magenta: GEOPHONE depository). The earthquakes with magnitudes greater 4.5 and occurred between 1997 and 2009 are selected.

of the earthquakes are located along the active seismic zones, North Anatolian Fault (NAF), East Anatolian Fault (EAF) and Aegean subduction zone. Fewer earthquakes were included from Caucases and Iran. The earthquakes along NAF and EAF have mostly strike-slip mechanisms while the majority of the events from the western Anatolia and Aegean have normal and strike-slip mechanisms. The range of the recording distances used for the surface wave analysis was between 600 and 2200 km.

4 SURFACE WAVE DISPERSION MEASUREMENTS

The surface wave dispersion curves were computed in several steps. The first step involved visual check of the waveform data to insure reasonable signal-to-noise ratios and eliminate problematic recordings. Radial and transverse components were computed by rotating NS and EW components into backazimuth directions. We obtained Love waves from transverse components and Rayleigh waves from vertical components. The instrument responses were removed from the selected waveforms and the waveforms were decimated to 5 samples per second.

We employed both MFA (Dziewonski *et al.* 1969; Herrmann 2002) and reassigned multiple-filter analysis (RMFA; Pedersen *et al.* 2003) to estimate the surface wave group velocities. RMFA is an improved interpretation of MFA. Rather than attributing the energy to the centre of the applied frequency and time windows, it is attributed to a location within the window that corresponds to the centre of gravity. Objective of the method is to improve the precision of group velocity measurements with energy reassignment in time-frequency domain (Pedersen *et al.* 2003). RMFA provides better-constrained dispersion curves than classical MFA that shows smeared image of group velocities especially at higher periods.

To test the accuracy of group velocity estimates we used both synthetic and recorded waveforms. Fig. 4(a) shows RMFA and the group velocity curve of the recording at AHLT station from an aftershock (Mw = 5.0) of 1999 November 12 Duzce (Mw = 7.2) earthquake (Fig. 2). Fig. 4(b) shows RMFA of a synthetic waveform for a crustal model obtained by a simple grid search based on the dispersion curve in Fig. 4(a). We used discrete wavenumber summation method (Herrmann 2002) to compute the synthetic waveform. The dispersion curve computed from the same model is also shown in Fig. 4(b) (Herrmann 2002). The computed group velocities using RMFA is in good agreement with the dispersion curve calculated from the crustal model (see Fig. S1).

We interactively picked group velocities from both MFA and RMFA. MFA provided better continuity at lower periods while RMFA provided increased resolution at greater periods. Two dispersion curves calculated from the two crustal models were used to guide the picks (Fig. 5). The first earth model with thick crust was determined from a simple grid search as explained above while the second earth model corresponding thin crust was obtained from Akyol *et al.* (2006) assuming a Vp/Vs ratio of 1.75. Using the group velocity picks we applied velocity filtering to the waveforms (Herrmann 2002) and recalculated RMFA of the velocity-filtered waveforms. Group velocity picks were revised and improved. Assuming that the wave follows the great circle arc between the source and the receiver, the group velocity for a given period was estimated by dividing the epicentral distance by the group arrival time. Standard deviations of group velocities were estimated from 95 per cent of group velocities.

© 2010 The Authors, *GJI*, **181,** 502–520
Journal compilation © 2010 RAS

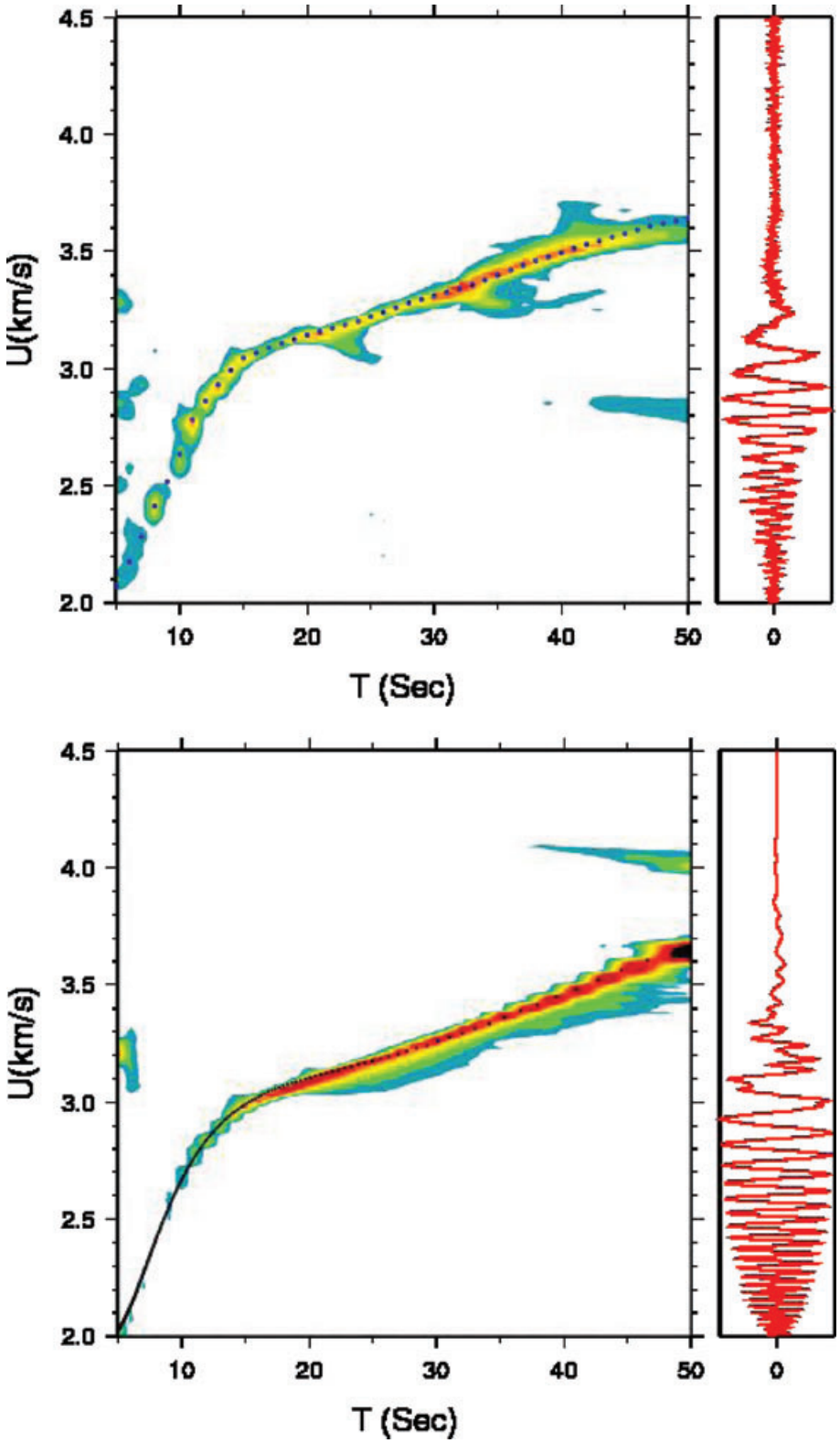

Figure 4. Analysis of waveforms using reassigned multiple-filter technique (RMFA). Top panel: RMFA (left-hand side) for the transverse component of the aftershock of Duzce earthquake (Fig. 2) recorded by AHLT station at $\Delta = 960$ km (right-hand side). The black dots on the top of the image show the group velocity picks. Bottom panel: RMFA (left-hand side) for the transverse component of the synthetic waveform (right-hand side) computed from the thick crust model (blue line) shown in Fig. 5. The black dots on the top of the image show the computed group velocities from the thick crust model. The colours indicate normalized energy at each period.

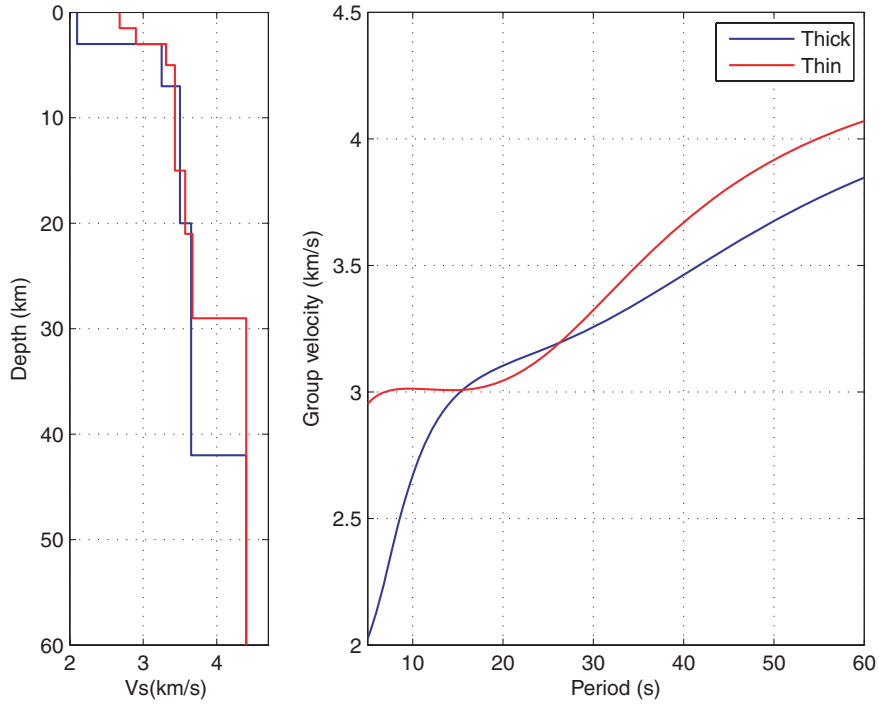

Figure 5. Dispersion curves (right-hand side) calculated from the end member crustal models (left-hand side) appropriate for the region (Blue: thick crust model, Red: thin crust model).

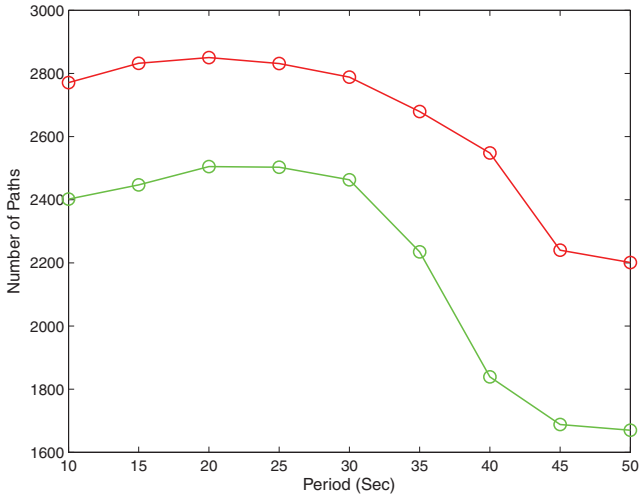

Figure 6. Number of Love-wave group velocity measurements at selected periods before (red) and after (green) the elimination of the paths with more than 20 s residual during tomographic inversion.

We initially computed MFA of 13 171 paths for both Love and Rayleigh waves. After applying a number of selection criteria approximately one forth of the paths provided reliable dispersion measurements for Love waves. The elimination of the dispersion curves was based on: (1) low signal-to-noise ratio of time domain signals, (2) the presence of no clear dispersion in the pre-defined range (8–50 s period), (3) complicated surface wave patterns resulting from multipathing and higher mode contributions, (4) the paths outside of the pre-defined distance range (600–2000 km), (5) the paths with traveltime errors greater than 20 s during tomographic inversion. Fig. 6 shows the number of Love-wave measurements at different periods after discarding the paths with epicentral distances outside of the pre-selected range and eliminating improper group velocity curves. Eliminating majority of the paths did not pose a significant problem on the resolution since the number of paths crossing grids is still sufficient.

Since the number of selected dispersion measurements for Rayleigh waves were found to be much lower than those of Love waves (about one-third of Love waves) the analysis was proceeded only using Love waves. It is worthwhile to mention that this observation is not consistent with the observations worldwide. We attribute this difference to the facts that: (1) the majority of the earthquakes used in this study have strike-slip mechanisms. It is well known that earthquakes with strike-slip mechanisms generate Love waves more efficiently than Rayleigh waves and amplitudes of Rayleigh waves attenuate faster at greater periods than Love waves (Tsai & Aki 1971; Aki & Richards 1980). Moreover, the amplitude spectra of Rayleigh waves usually have spectral holes, which can affect the continuity of dispersion curves (Tsai & Aki 1971). When we reduce the magnitude threshold of the earthquakes to $M\mathrm{w} = 4.5$ the amplitudes become an important factor for a higher signal-to-noise ratio. (2) The vertical component of surface waves is more affected by free surface topography than horizontal components. Turkey is surrounded by sea on three sides, high mountain ranges on the north and south. Such elevation differences may distort propagation paths and introduce scattering.

5 TOMOGRAPHY

To obtain group velocity maps we utilized a method proposed by Pasyanos (2005). The study region is divided into equal-area cells and the following system of equations is obtained:

$$\mathbf{t} = \mathbf{Ds}, \tag{1}$$

$$\lambda \mathbf{Ls} = 0, \tag{2}$$

© 2010 The Authors, *GJI*, **181,** 502–520
Journal compilation © 2010 RAS

where, **t** is a vector of surface wave group arrival times, **D** is a matrix containing the distances travelled in each cell and **s** is a vector of group velocity slowness. Eq. (2) imposes the smoothness constraint on the model parameters by constructing two dimensional Laplacian operators **L** of the slowness. The damping factor of λ controls the trade-off between fitting the traveltimes and smoothing the model. The inversion does not strongly depend on the initial velocity model. However, a fine grid could create regions with low or no ray coverage. Pasyanos (2005) proposed a variable smoothing operator to improve the resolution when the ray density is higher. We applied a variable smoothing operator with a multistep process for the inversion. A larger grid size was adopted at the first step with a constant initial model resulting in a low-resolution solution. The grid size was halved in the second step with the initial model obtained in the previous step.

The resolution is also a function of the path density, azimuthal distribution and average path length of rays. A number of tests using both real and synthetic data were performed to select optimum cell size and smoothing parameters. Fig. 7 shows ray hitcount and ray path coverage and Fig. 8 checkerboard tests to determine the effect of path coverage on the solution. The initial checkerboard models contained alternating velocity values of 3.0 and 3.5 km s^{-1} for low- and high-velocity regions. We performed tests with 4°, 2° and 1° input patterns. We started with a grid size of 2°, then computed image with 1° grid size. The final image was estimated with 0.5° grid size. Both the magnitudes and the shape of the rectangular patterns

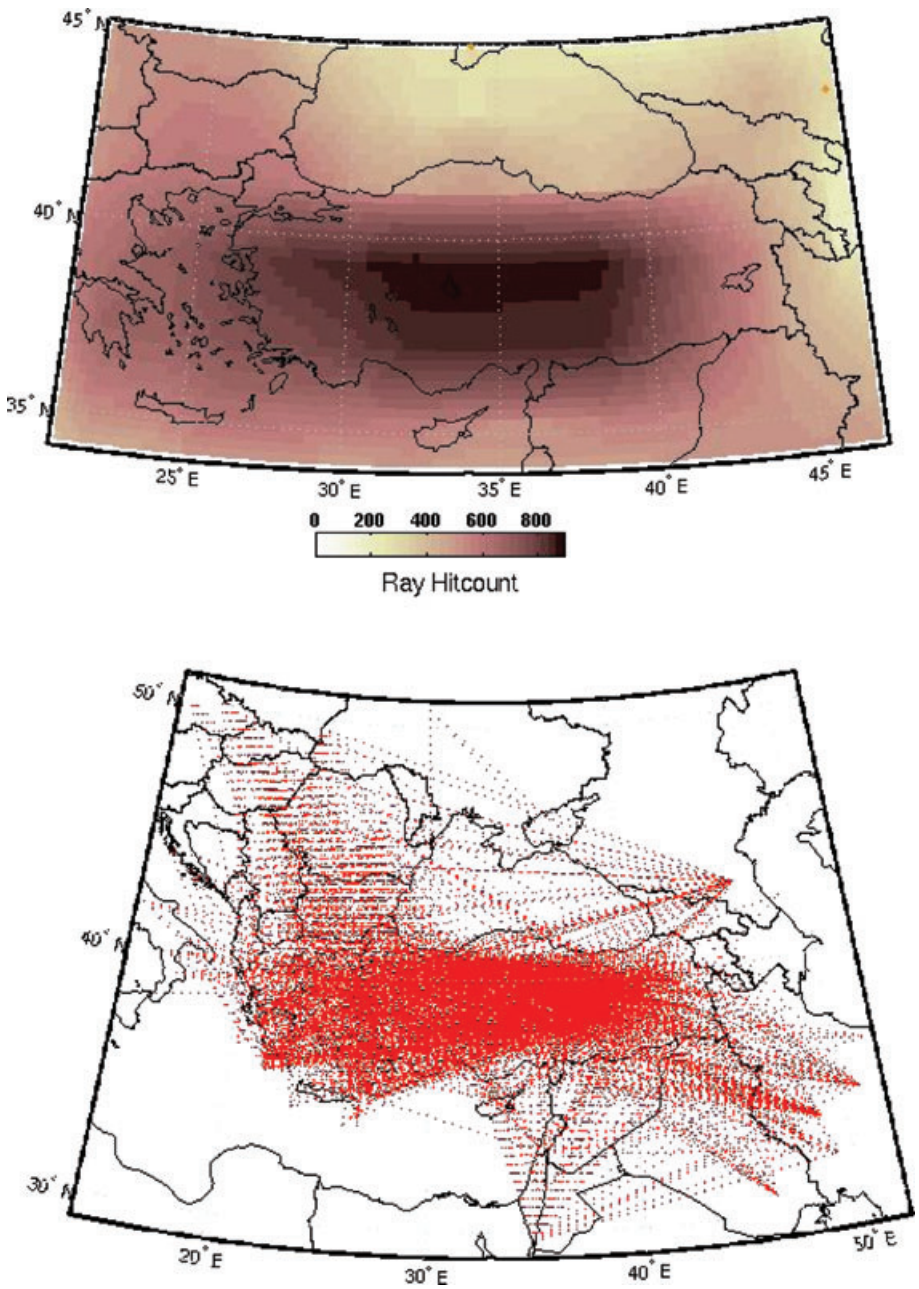

Figure 7. Ray hitcount (top panel) and ray paths (bottom panel) computed from 20 s period group velocity measurements for the final inversion run after the elimination of the paths. The cell size for the hitcount is 0.5°. The hitcount map and ray paths can change at different periods.

© 2010 The Authors, *GJI*, **181,** 502–520
Journal compilation © 2010 RAS

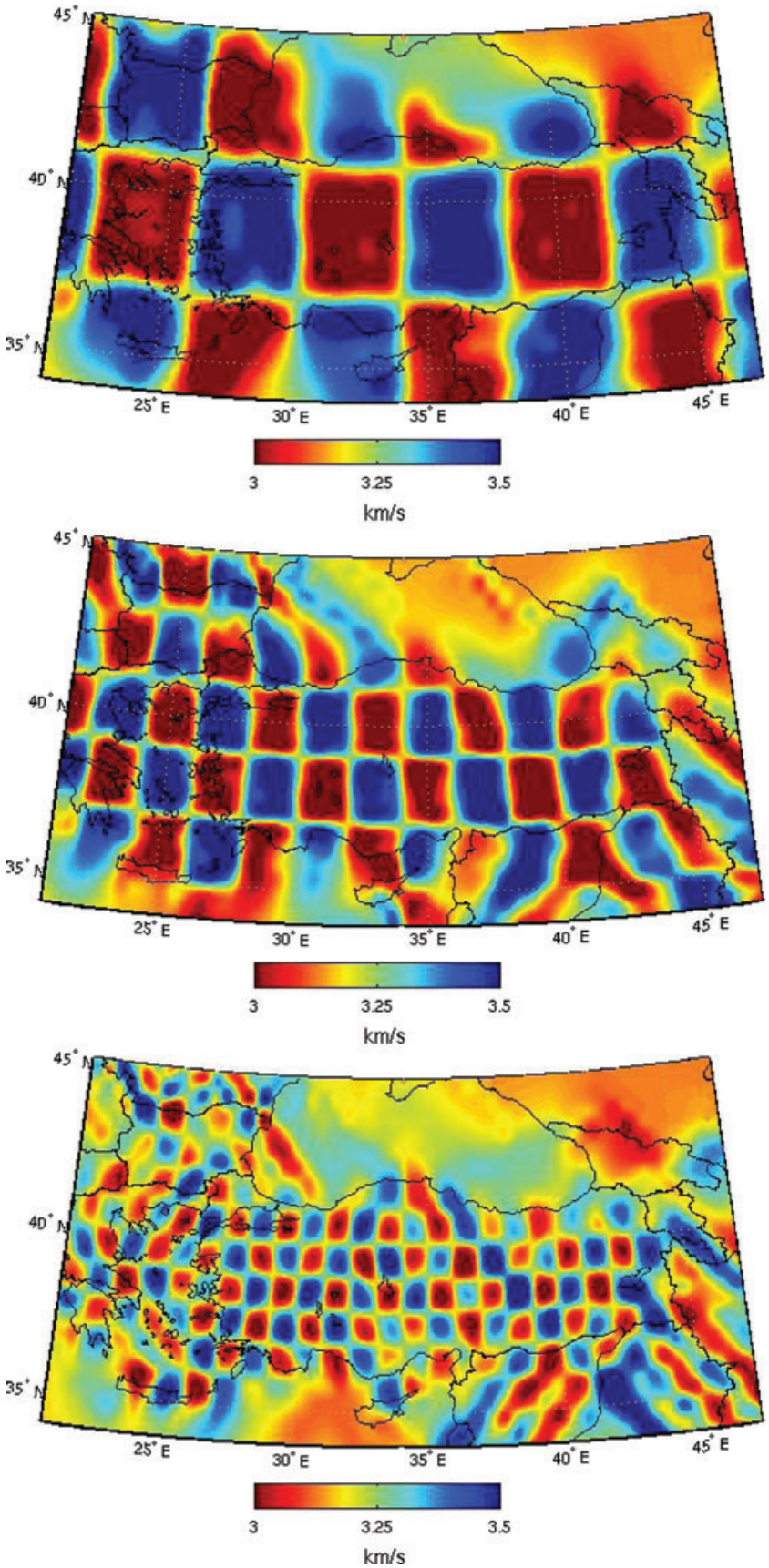

Figure 8. Checkerboard resolution tests using the path coverage of 20 s Love waves. Three types of input patterns with 4° (top panel), 2° (middle panel) and 1° (bottom panel) are tested.

© 2010 The Authors, *GJI*, **181,** 502–520
Journal compilation © 2010 RAS

were recovered in the majority of Turkey for 4°, 2° and 1° patterns (Fig. 8). The results are consistent with the path densities shown in Fig. 7. The resolution degrades for 2° and 1° patterns outside of Turkey with poor ray coverage, especially in the Black Sea and the Mediterranean Sea. In the Arabian plateau the smearing of the patterns also indicates insufficient ray coverage. Structures smaller than 2° cannot be resolved in the areas with low ray coverage. Such areas are located along the Black Sea coast, Hellenic arc and the Mediterranean coast. However, the long wavelength features (>2°) can still be recovered in majority of the domain with the exception on the northern part of the Black Sea. The checkerboard tests only indicate if the path coverage is sufficient. Therefore, we performed an additional test to determine the effect of the spatial sampling on the inversion. We randomly selected 50 per cent of the paths with replacement and determine the outcome of the initial checkerboard pattern after several inversion runs. The results were consistent with the full checkerboard test with complete database indicating that the number of paths used during the inversion is sufficient to attain the desired resolution.

Group velocity maps of Love waves were computed in few steps. We initially obtained smooth group velocity maps at each period to identify and discard group velocity measurements with traveltime residuals larger than 20 s (Fig. 9). We then computed final group velocity maps in three steps as explained during the checkerboard test. We estimated group velocity maps with 2° grid interval and then use the resulting maps as the input model to compute maps with 1° grid spacing. Final images were calculated for 0.5° grid interval.

There are additional concerns beside the path distribution, weighting of the data and spatial smoothing that may affect the

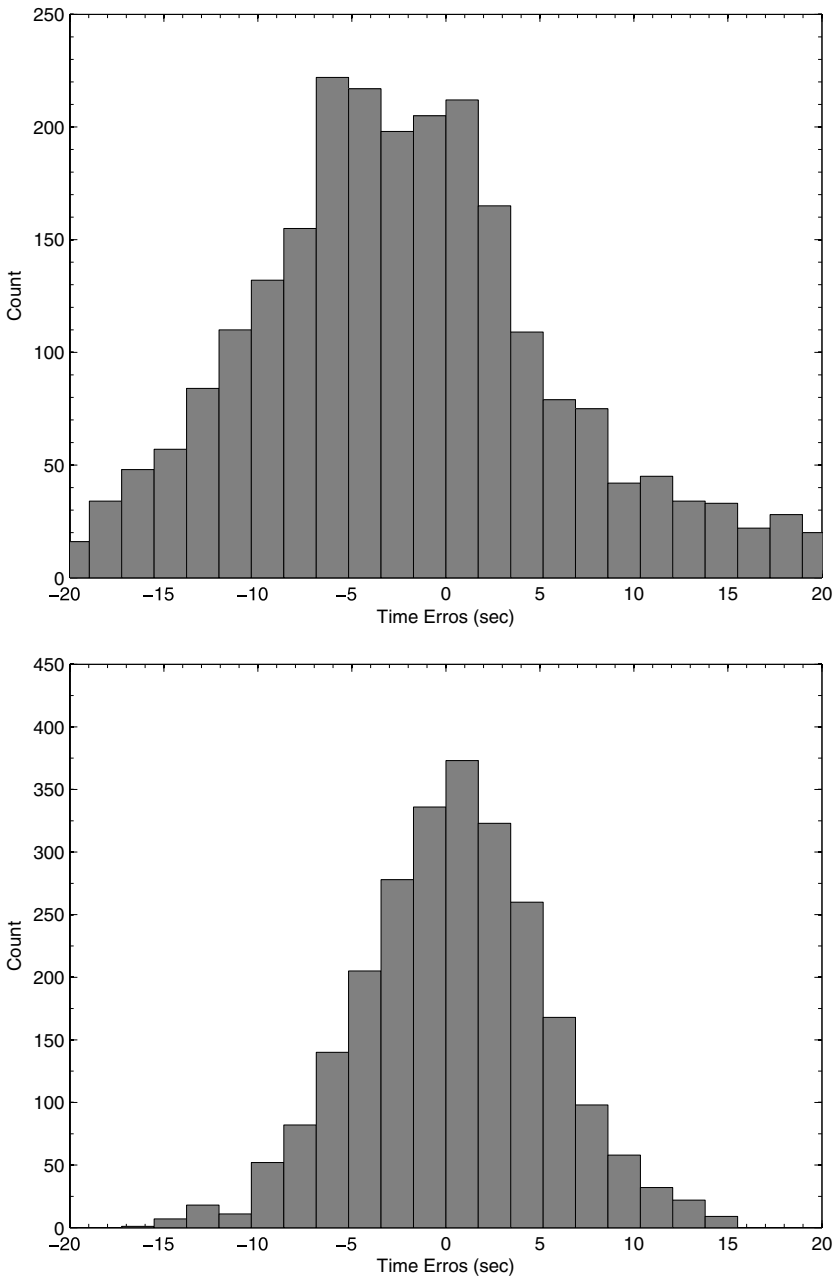

Figure 9. Histograms of traveltime misfits for initial model (top panel) and final model (bottom panel) at 20 s period.

© 2010 The Authors, *GJI*, **181,** 502–520
Journal compilation © 2010 RAS

resulting maps. These are (1) location errors of the earthquakes, (2) distortions in 3-D wavefields due to lateral inhomogeneities, (3) anisotropy (Vdovin *et al.* 1999). The earthquakes selected for the group velocity dispersion measurements were also relocated using the available data. The hypocentral errors of the earthquakes in Turkey are less than 5 km. However, the estimated errors for the events outside of the network coverage may reach 10 km. These values will have negligible effects on the estimated traveltimes for the distance ranges used in this study.

The assumptions made in the formulation of tomography problem contain significant simplifications. The effect of anisotropy and deviations from straight ray paths are totally ignored in this study. It is well known that ray theory is a high-frequency approximation, which is not justified in the presence of large lateral heterogeneities. For the ray approximation to be valid, the first Fresnel zone must be smaller than the scale-length of the heterogeneity, which places limitations on the lateral resolution of seismic models based on ray theory (Levshin *et al.* 2005). Such effects are not investigated in this study and may have varying degrees of importance when large lateral velocity contrasts exist.

6 GROUP VELOCITY MAPS

Using the tomographic inversion method as described in the previous section, Love-wave's group velocity maps at 10, 15, 20, 30, 40 and 50 s were computed. Group velocity maps were produced for several smoothing parameters, $\lambda = 50, 100, 200$. We preferred to use the value of $\lambda = 200$, which gives relatively smooth maps with small solution errors. The rms traveltime errors for the initial and final velocity maps at different periods are listed in Table 1. We also computed histograms corresponding to traveltime errors at each step for initial and final group velocity maps. Fig. 9 illustrates histograms for the traveltime errors at 20 s period. The histograms show that the misfit for the data meets the criteria that eliminate traveltimes errors greater than 20 s.

We computed sensitivity kernels of Love waves to determine how the structure in a certain depth interval influences the group velocities. These functions are the partial derivatives of group velocity with respect to a perturbation of shear wave velocity in the reference model through which they are computed. Fig. 10 shows the sensitivity kernels for two earth models at a number of periods. Slowly varying sensitivities of Love waves limit the depth resolution and mask deeper structures. The shallow structures dominate at lower periods and have significant influence at higher periods. Vdovin *et al.* (1999) indicated that group velocity maps will have positive correlation with shear wave anomalies or boundary topography in the neighbourhood of the positive maximum of the sensitivity kernel. The reason is that the negative values in the sensitivity kernels has lower amplitudes and is more limited in depth extent.

At 10–15 s Love waves mainly sample the upper crust of 10 km thickness. Waves with 20 s period are more sensitive up to a depth of 20 km and therefore contain information on both upper and lower crust. Intermediate periods (20–40 s) sample the crust more uniformly and are influenced by the upper-mantle velocity for a crustal thickness of 28 km. At greater periods (>40 s) the low group velocities result mainly from thickened crust. The influence of upper mantle is apparent for crustal thickness less than 30 km when there is no significant masking from thick sedimentary basins.

Group velocities at 10–15 s are sensitive to upper crust and influenced by local sedimentary basins and topographical features (Figs 11a and b). Several inland and offshore basins exist in Turkey (e.g. Thrace basin, Cilicia–Adana basin, Tuz Gölü basin, Sinop–Boyabat basin, Marmara Sea, Black Sea and Aegean Sea and Mediterranean Sea, Black Sea basins). Low group velocities are observed in the Marmara Sea, Thrace basin, Saros Bay, Sinop basin, Black Sea and Mediterranean Sea, indicating the presence of thick sedimentary deposits. Low group velocities observed in the eastern Anatolia take place at a region with widespread volcanic activity.

As indicated by the sensitivity kernels the group velocities at 20–30 s periods are influenced by a thickness of 20–25 km (Figs 11c and d). As a result, we observe anomalies associated with geological structures at crustal scale. Group velocities are higher along the Pontides, IZ, Strandja massif on the north of the Izmir–Ankara–Erzincan suture zone. High group velocities are observed in central Anatolia, Hellenic arc and Menderes massif. The collision belt in Bitlis suture is characterized by high group velocities. A larger velocity contrast exists between high group velocities in the BM and low group velocities in the eastern Anatolia. Low group velocities are observed in Antalya Bay, west of Cyprus, with a continuation towards the IA. A wedge-shaped anomaly in the IA is a prominent feature on the group velocity maps starting from 10 s period. The low group velocities observed in the Black Sea can be associated with two deep basins. Low velocities observed in the western Black Sea basin extend to Moesian Basin. However, both the geometry and magnitude of these anomalies may have significant uncertainties due to poor ray coverage.

Group velocities at 40 and 50 s are influenced by the lower-crust and upper-mantle structure (Figs 11e and f). In this period range the wavelengths of the anomalies on the maps are larger with smaller velocity perturbations. The central Anatolia and Taurides have more uniform distribution of group velocities. High group velocities are observed in the Aegean region, Rodophe–Strandja massif, eastern Pontides and Bitlis suture zone while the low group velocities appear in the eastern Anatolia, the Antalya basin and the IA.

Using the group velocity maps of Love waves at different periods obtained from tomography, local group velocity curves for the stations shown in Fig. 2 are constructed (Fig. 12). Dispersion curves indicate that there is a good continuity of tomographic images of increasing periods. They also show the geographical variations of the crustal structures in the area. However, the influence of the upper mantle is not apparent on the curves indicating measurements at

Table 1. Number of observations used for the tomographic images, values of the initial and final group traveltime residuals and standard deviations for different periods.

Period (s)	Number of Observations	Initial error (s)	Standard Dev (s)	Final error (s)	Standard Dev (s)
10	2402	20.1	28.9	10.5	10.1
15	2447	12.1	20.1	5.7	8.0
20	2505	8.9	15.2	4.1	5.9
30	2463	7.3	10.2	3.4	4.6
40	1839	6.5	8.6	3.4	4.3
50	1670	4.8	6.0	3.2	4.0

© 2010 The Authors, *GJI*, **181,** 502–520
Journal compilation © 2010 RAS

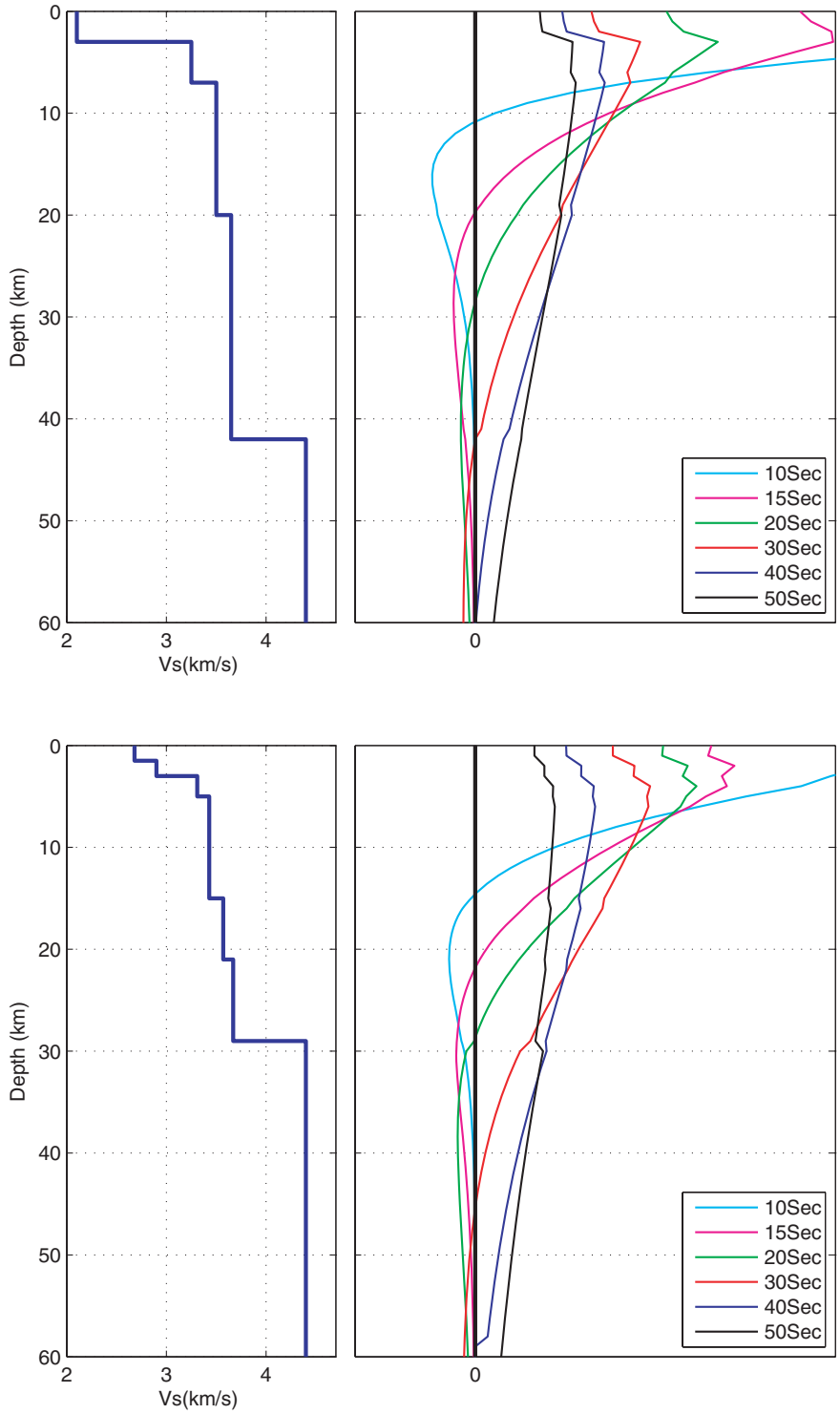

Figure 10. Shear wave sensitivity kernels of Love waves at periods ranging from 10 to 50 s for a shear wave velocity-depth function using two crustal models displayed in Fig. 5.

greater periods are necessary. The curve with lowest group velocities is obtained for the station ANTB located in Antalya Bay while the curve with the highest group velocities is observed at station BALB in the western Anatolia.

Fig. 13 show the tomographic images at 25 s with major tectonic units, suture zones along with the volcanism. At 25 s period Love waves sample upper and lower crust and are also influenced by the upper mantle with a crustal thickness of less than 25 km. Major geological and tectonic boundaries and features can be identified with velocity contrasts along the boundaries. The volcanisms observed in various areas of the region have different origins, therefore located both on the high and low velocity anomalies.

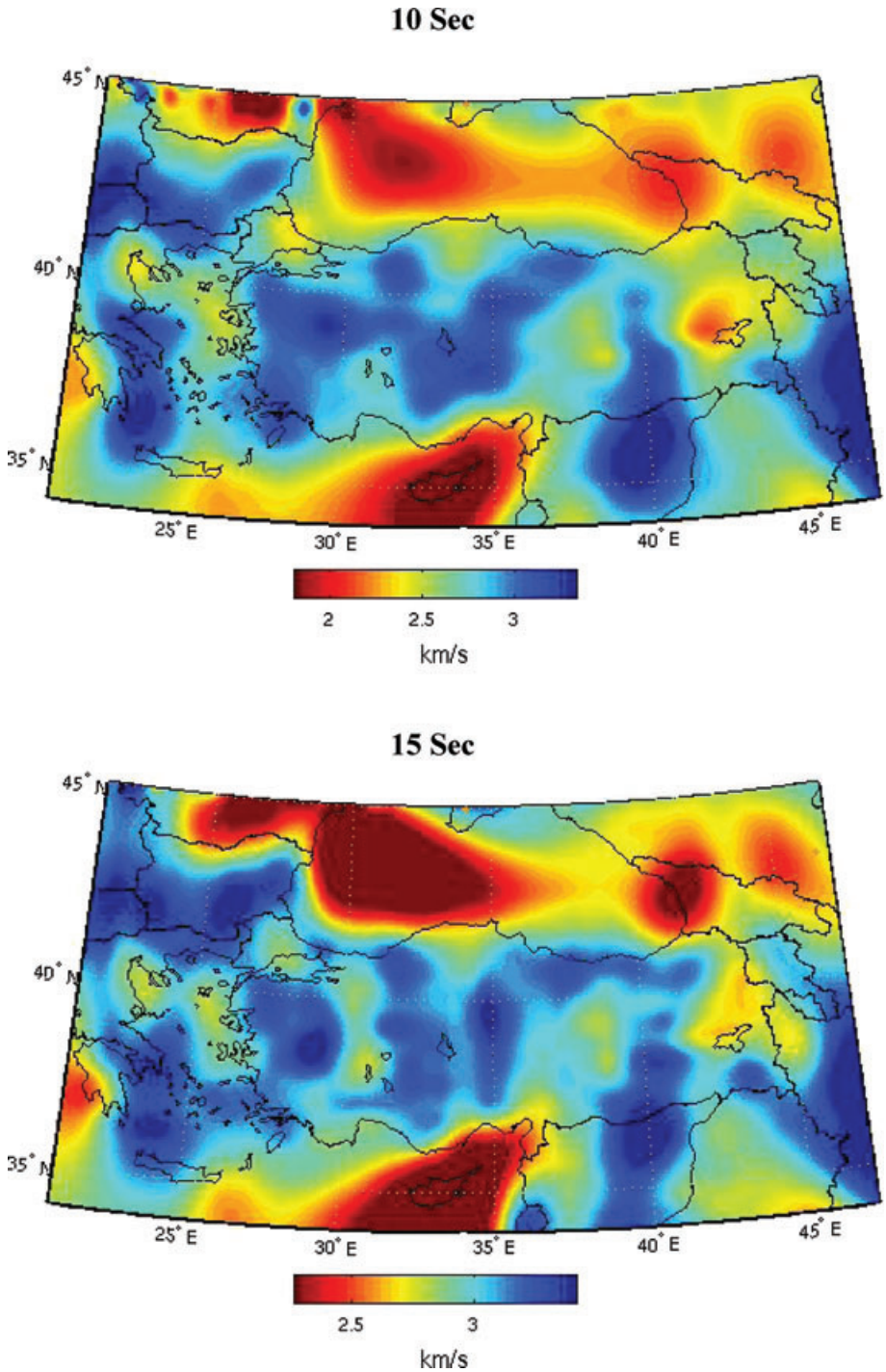

Figure 11. a–f. Estimated Love-wave group velocity maps at 10, 15, 20, 30, 40 and 50 s periods.

7 DISCUSSIONS AND CONCLUSIONS

Love-wave group velocities in Turkey and the surrounding regions were measured from the local and regional earthquakes recorded at a large number of stations. We obtained Love-wave group velocity maps between 10 and 50 s periods using a tomographic inversion method. The maps indicate the presence of significantly different crustal compositions and structures resulting from different tectonic evolutions. Group velocity maps exhibit strong velocity perturbations and correlate well with the known tectonic structures. In general, the tomographic images at short periods (10–15 s) displaying low velocities associate with the sedimentary basins, intermediate periods (20–30 s) with regional geologic structures and greater periods (40–50 s) with total-crustal structure and upper mantle.

In the following part we present the results of this study and compare to the previous works.

7.1 Marmara and the northern Aegean

Sedimentary basins in the Marmara Sea manifest themselves on the maps by low group velocities at 10–15 s periods (Figs 11a and b). The recent seismic reflection studies show three deep basins in the

© 2010 The Authors, *GJI*, **181,** 502–520
Journal compilation © 2010 RAS

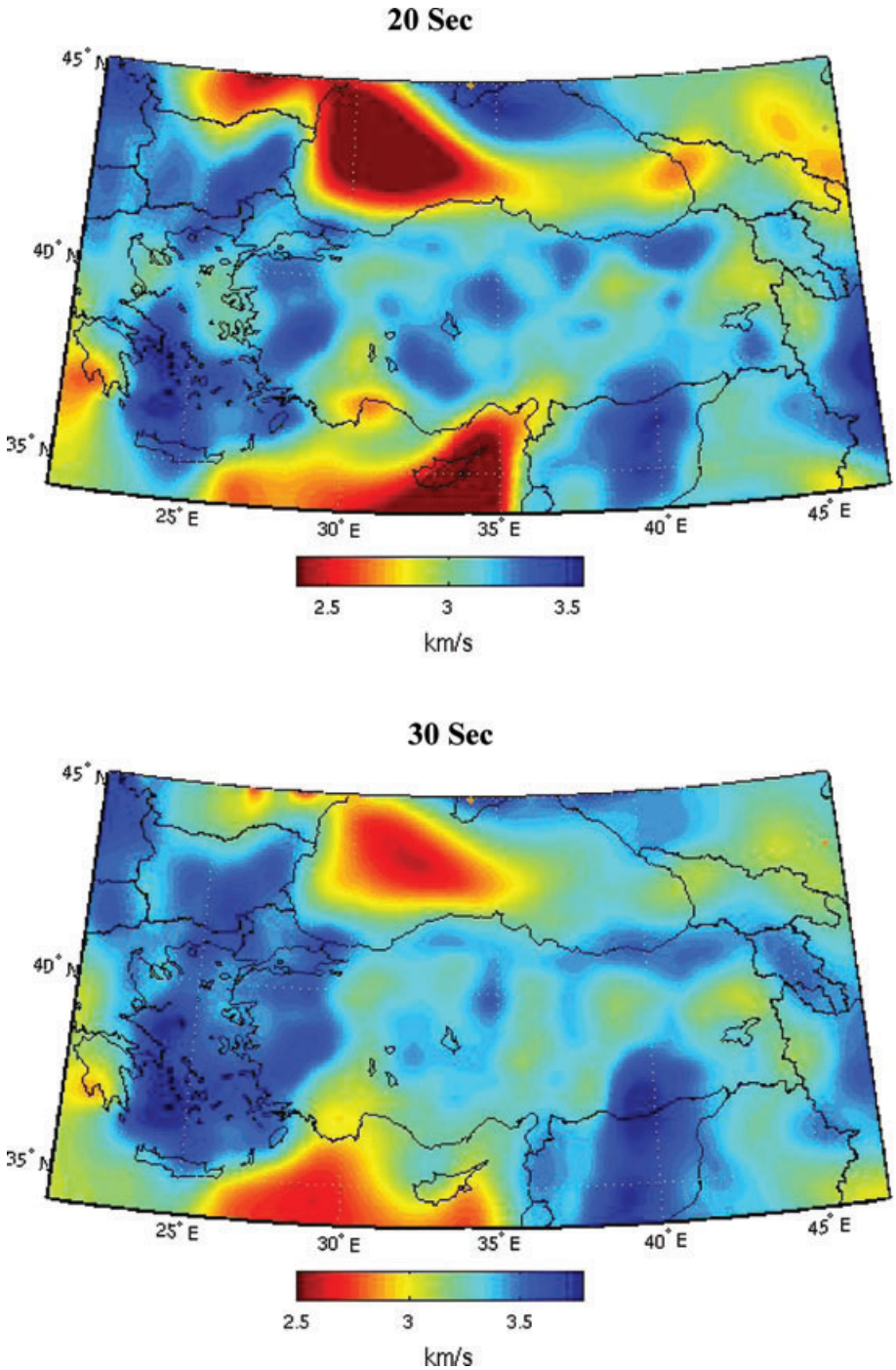

Figure 11. (*Continued.*)

Marmara Sea exceeding 5 km of thickness (Laigle *et al.* 2008). The basins are filled with low velocity sediments overlying high velocity basement of the IZ characterized by Paleozoic units. The low group velocities observed in the Marmara Sea are extending to Thrace Basin, which is the largest and thickest Tertiary sedimentary basin in Turkey with a sedimentary fill reaching to a depth of 9 km. The basin on the north is bordered by metamorphics and granites of the Stranjia Massif, which are characterized by high group velocities on the maps. Laigle *et al.* (2008) obtained the crustal thickness in the sea of Marmara as 26 km. The results of receiver function analysis indicate a crustal thickness of ∼30 km on the north of Marmara Sea and increasing to ∼34 km on the south (Zor *et al.* 2006). Therefore, significant local variations on the Moho topography are proposed. We observe group velocities increasing at 25 s period and reaching to the regional values surrounding the Marmara Sea. The sensitivity kernels in Fig. 10 for a crustal thickness of 30 km indicate that the influence of upper mantle starts at 30 s period. Therefore, it is reasonable to expect that the thickness of the crust is less than 30 km in the Sea of Marmara to explain observed higher group velocities.

Lower group velocities are also observed in the Saros bay, on the west of the Marmara Sea and elongating towards the North Aegean

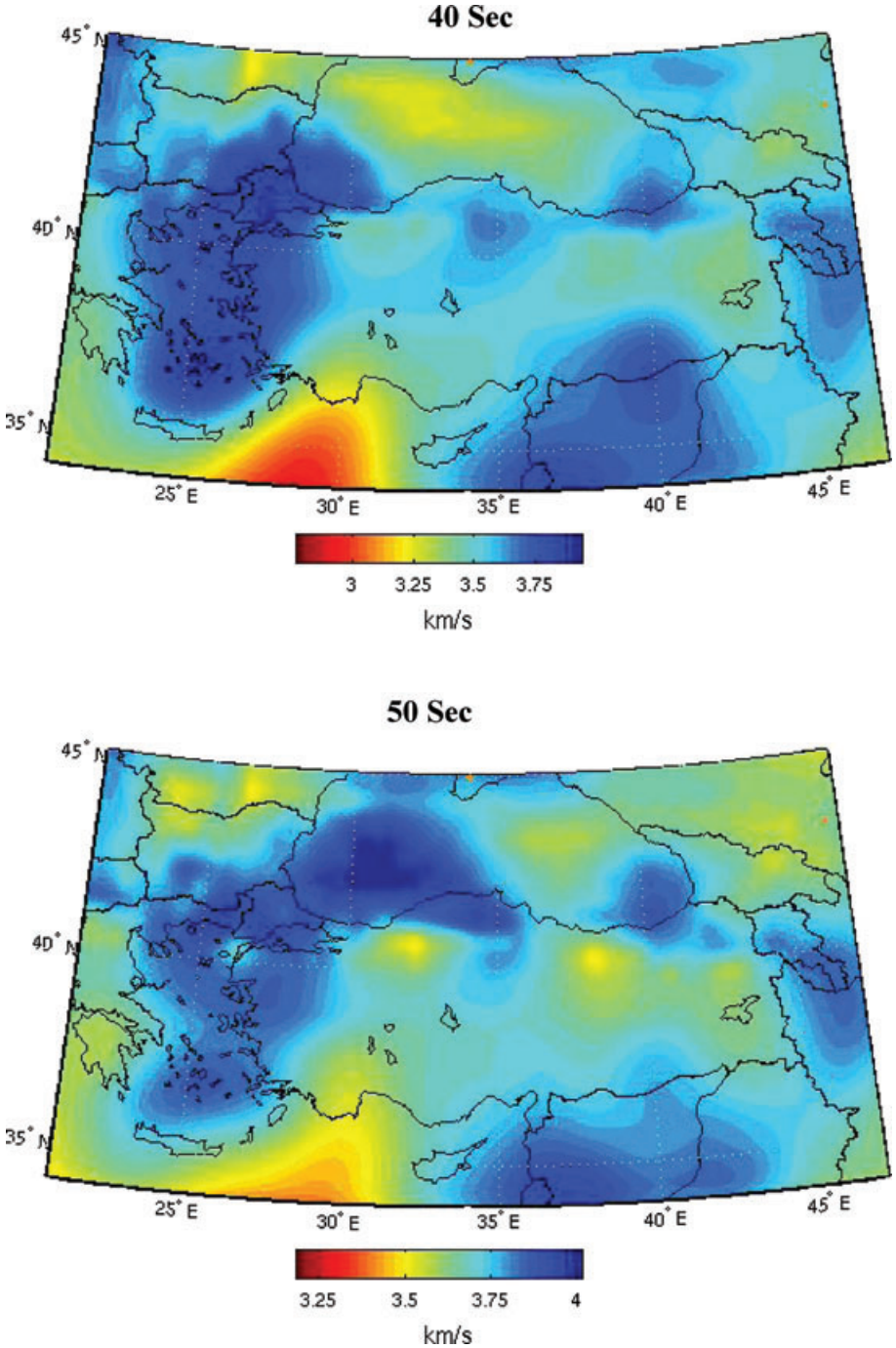

Figure 11. (*Continued.*)

Trough and the Axion basin (Figs 11a and b). Karagianni *et al.* (2002) also observed low group velocities of Rayleigh waves along these transtensional basins which are controlled by the NAF of strike-slip character and the Aegean tectonics of extensional nature. The thickness of the sediments in these basins is expected to reach up to 6 km (Karagianni *et al.* 2002).

The Rodop–Stranjia massif on the north of the Aegean Sea appears with higher group velocities at all periods (Figs 11a and e). This indicates high crustal velocities, which are related to metamorphic and plutonic rocks. The high velocities along the Rodop–Stranjia massif have the continuity on the north of the Marmara region.

7.2 Aegean Sea and the western Anatolia

High group velocities on the north of the Hellenic arc in the Aegean Sea appear from 10 s periods. The values in this part of the images do not correlate with Karagianni *et al.* (2002). This can be related to poor ray coverage in this study. On the other hand, the western coast of Anatolia exhibits low velocities on 10–15 s maps. Similar

© 2010 The Authors, *GJI*, **181,** 502–520
Journal compilation © 2010 RAS

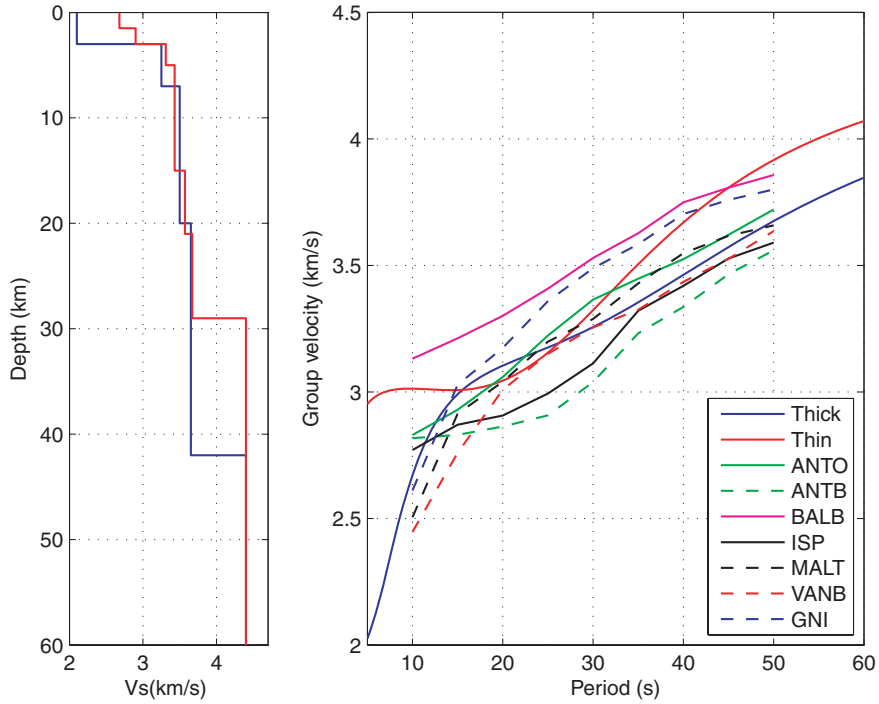

Figure 12. Local dispersion curves derived from the group velocity maps at five seismic stations shown in Fig. 2. Dispersion curves computed from thin and thick crustal models are also shown.

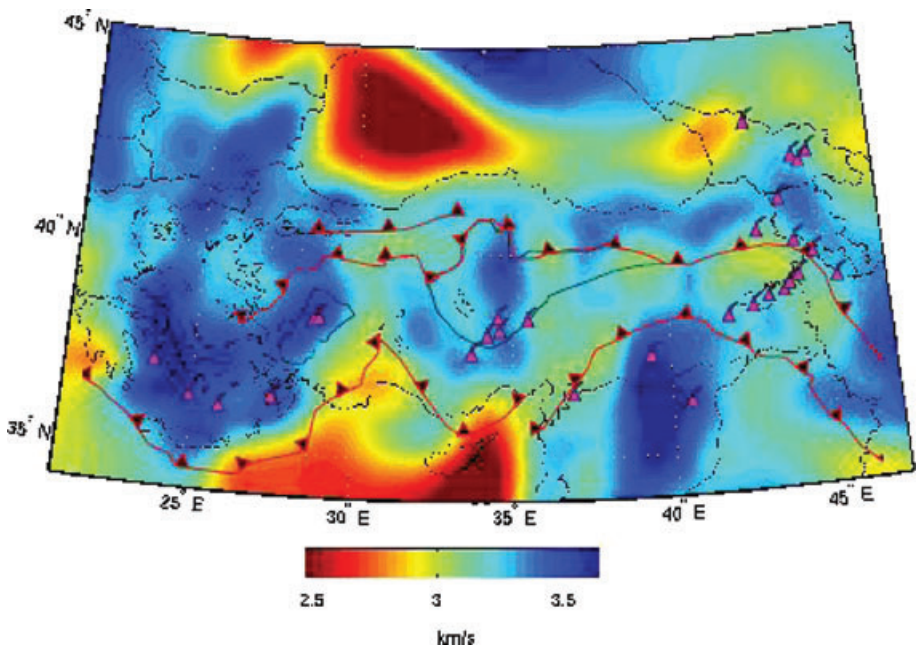

Figure 13. Estimated Love-wave group velocity maps at 25 s period with major tectonic units, suture zones, neogene and quaternary volcanoes.

distribution of group velocities is observed by Karagianni *et al.* (2002). Low group velocities are related to the sedimentary layer in the Aegean Sea. DiLuccio & Pasyanos (2007) observed a progressive increase in the sediment thickness from the northern Aegean (3–5 km) to the north of Creete (∼10 km). However, the low velocities in the North Aegean Trough and Saros Bay are persistent even at 20 s period. This may be an indication of crustal thickening from the southern Crete towards the northern Aegean Sea. Sensitivity kernels in Fig. 10(b) show that group velocities at 20 s period begin to be influenced by a thickness of greater than 20 km. Moho depths for the Aegean Plate computed by Sodoudi *et al.* (2006) indicate that the southern part of the Aegean has a crustal thickness of 20–22 km while the northern Aegean Sea shows a relatively thicker crust (25–28 km). Similar values were obtained by DiLuccio & Pasyanos (2005) indicating an increase of crustal thickness of 20–25 km in the southern, central-western Aegean, whereas

reaching 32 km in the northern Aegean. Such differences in the crustal thicknesses has been interpreted that the extension strongly influenced the southern Aegean while presently undergoing high crustal deformation in the northern Aegean Sea (Sodoudi *et al.* 2006).

Significant velocity contrast exists between low group velocities in the Aegean Sea and high group velocities of the western Turkey. The contrast also appears on the Rayleigh wave maps of Karagianni *et al.* (2002) between 6 and 19 s. The observed contrast is the result of low velocity sediments of the Aegean and high velocity metamorphic core complex in the region (e.g. Menderes Massif). The contrast disappears at periods greater than 25 s indicating the influence of the lower crust and upper mantle. However, a velocity contrast appears between the western Anatolia and the central Anatolia at 29°E indicating a thicker and slower crust. A gradual thickening of the crust is observed from the Aegean to the western Turkey from 25 to 32 km and reaches to ∼40 towards the central Anatolia (Karagianni *et al.* 2005; Zhu *et al.* 2006; DiLuccio & Pasyanos 2007).

7.3 Southern Anatolia and IA

One of the prominent features of the group velocity maps is the presence of a wedge-shaped low-velocity anomaly in the Antalya Bay elongating towards the IA. Low velocities start appearing at 10 s map and continue to be present at greater periods with increasing wavelengths. The low velocity anomaly of IA is delimited by the Menderes massif in the west and the Sultandag–Beysehir massif in the east. In the centre of IA, a regional allochthonous unit, Antalya complex, represents a critical part of the evidence of a southerly Neotethyan oceanic basin (Robertson 2000). Several carbonate platforms, sedimentary basins and ophiolits exist in this complex. The deep structure of Antalya Bay, the offshore extension of the IA, is poorly known. Earthquake locations suggest the existence of a detached oceanic slab beneath the Antalya bay even though the timing and the geometry of the slab remains unclear (Engdahl *et al.* 1998; Robertson 2000). The crustal thickness obtained from receiver function analysis at ISP station, which is located within IA is found as 42 km, significantly thicker than 35 km of ANTO station (Zhu *et al.* 2006). This indicates significant crustal thickening as a result of collision. DiLuccio & Pasyanos (2007) observed crustal thickening from 30 km near Cyprus to 50 km in the central Turkey with lower crustal velocities. The 2–3 km thick soft sediments presented on their maps can be related to the allochthonous units in IA and appear on 10–20 s maps of this study while at greater periods (40–50 s) slower velocities indicate a thicker crust.

Low group velocities at 10–15 s appear in the Cilicia–Adana basin located between Turkey and the northern Cyprus. The seismic reflection data show that this basin contains sediments with 3 km thickness (Aksu *et al.* 2005). The lower sections of the Cilicia–Adana basin were not imaged by the seismic reflection data but expected to contain a thicker sedimentary sequence. The low group velocities observed on 10–20 s maps also support the presence of a thicker sedimentary basin. Anomalously low velocities associated thick layers of sediments on the west of Cyprus were observed by DiLuccio & Pasyanos (2007) while relatively higher velocities and thinner sedimentary section were found on the east of Cyprus. In contrast we observed high group velocities in the east of Cyprus for 10–20 s periods indicating the presence of thick sedimentary column.

7.4 Eastern Anatolia

A prominent low velocity anomaly on the 10–30 s group velocity maps appears in the Eastern Anatolia region surrounded by higher velocities of the eastern Pontides and the collision zone of Anatolia-Arabian plates. Şengor *et al.* (2003) and Keskin (2003) proposed that the eastern Anatolia region can be characterized by three tectonic units; the Pontides on the north, in the centre the Eastern Anatolian Accretionary Complex (EAAC) and collision-related volcanics and finally on the south Bitlis–Pötürge massif.

The eastern Pontides characterized by higher group velocities are considered as a magmatic arc of Albian to Oligocene age. Its basement is represented by a metamorphic massive named the Pulur Complex (Topuz *et al.* 2004). The magmatic arc formed by a north-dipping subduction under the Eurasian continental margin (Yılmaz *et al.* 1998; Sengor *et al.* 2003). Along the suture zone separating the Pontides from Anatolian–Iranian platform ophiolits, mélanges and forearc deposits are exposed. There is a gradual crustal thickening along the Pontides starting at 32 km in the western Pontides and reaching to 44 km in the eastern Pontides (Mooney *et al.* 1998). Crustal thickening and initiation of volcanic activity started as a result of subduction-related compression and consumption.

As Şengor *et al.* (2003) and Keskin (2003) suggested, the EAAC is produced by the consumption of the Neo-Tethyan ocean and a widespread volcanic activity from upper Miocene to Quaternary was observed in the region with the complete elimination of the Neo-Tethyan ocean floor as a result of collision between Arabia and Eurasia during Early Miocene (Yılmaz *et al.* 1998). The volcanism started earlier in the north and migrated to the south as a result of the slab steepening under the eastern Anatolia region. Several tectonic models have been proposed to explain the subduction and post-collisional evolution of the region. Based on the crustal thickness (Zor *et al.* 2003), low *Pn* velocities (Al-Lazki *et al.* 2003) and high *Sn* attenuation (Gök *et al.* 2003), Keskin (2003) and Şengor *et al.* (2003) proposed the absence of the subducting Arabian Plate beneath the Anatolian plateau. They suggested that the lithospheric mantle is either thinned or totally removed in the region. Keskin (2003) also proposed that the interaction of hot asthenosphere with the EAAC that contains retained water decreases the melting temperatures at a giving depth, generating extensive melting in the crust. Such interaction can account for the variability of lava chemistry and magma–crust interaction as well as low velocity zones observed in this study. The shallowest Curie point depths are observed in the area of the Quaternary volcanism and correlates well with the observed low-velocity zones (Aydın *et al.* 2005). The shallow Curie point depths imply that the magma source causing the low-velocity zones is located at shallower crustal depths.

At greater periods (>30 s) we still observe lower group velocities in eastern Anatolia. The average crustal thickness is varying from 38 km from the Arabian platform to 50 km in the Pontides with a regional average of 45 km (Gök *et al.* 2007). Therefore, we do not expect the influence of upper mantle at 50 s. The low group velocities were also observed on the tomographic images presented by Gök *et al.* (2007). They observed low *S*-wave velocities in the eastern Anatolia and high velocities on the Arabian foreland.

7.5 Central Anatolia

The KM located in the central Anatolia does not appear as a uniform velocity block on 10–20 s group velocity maps. Higher group velocities are observed in the core of the massif and relatively lower velocities in the area of the Tuz Gölü basin. However, at greater

© 2010 The Authors, *GJI*, **181,** 502–520
Journal compilation © 2010 RAS

periods (40–50 s) the group wave velocities have more uniform distribution. This indicates that the heterogeneities are confined to the upper crust in the massif. The KM is regarded either as the metamorphized northern margin of A–T terrain or a distinct terrane separated from A–T by the Inner Tauride suture. The massif contains oceanic remnants derived from the Neo-Tethys Ocean, which separate them from the Sakarya continent. It is considered to represent variably tectonized and subducted oceanic lithosphere and continental carbonate platform that were subsequently ejected from an accretionary–subduction complex on the collision with the Sakarya microcontinent (Floyd *et al.* 2000). The present seismicity of Turkey indicates that internal deformation of the central Anatolia appears to be less than eastern and western Anatolia. Therefore, it is not surprising to expect a more rigid and homogenous lower crust. We do not observe an obvious correlation between group velocities and volcanism in the central Anatolia in contrast to the eastern Anatolia. This indicates that the origin of the volcanism in the central Anatolia is significantly different from the eastern Anatolia.

7.6 Black Sea

Two distinct group velocity anomalies appear in the Black Sea starting at 10 s period. Although additional ray coverage is necessary to increase the reliability of the maps the features with larger wavelengths ($>2^\circ$) can still be associated with the known geological features. The Black Sea is composed of two deep basins. The western Black Sea basin has a maximum thickness of 19 km while the eastern Black Sea basin has 12 km of thick sediments. There is a significant crustal thinning (up to 10 km) below these basins with a total crustal thickness of 20 km (Spadini *et al.* 1996). We do not clearly observe the effect of crustal thinning on the group velocity maps. The low-velocity basins mask the deeper structures, which can be observed from the slowly varying sensitivities of Love waves.

Based on the group velocity maps we divided the area into five distinct regions. The Anatolian block displays a heterogeneous upper crust at 10–20 s periods while low group velocities at larger periods (>30 s) indicate more uniform lower crust. The low group velocities observed at larger periods can be related to low crustal velocities and/or thicker crust. Love waves at 50 s period are not significantly influenced by a crustal thickness of greater than 35 km. Significant velocity contrasts are observed between the Anatolian block and the surroundings indicating variations on the crustal types and tectonic styles. The Aegean region in the west is characterized by high group velocities as a result of crustal thinning. The Pontides on the north exhibit high group velocities as a result of high crustal velocities and crustal thickening from east to west along the Black Sea coast. The Mediterranean region on the south is characterized by very low group wave velocities as a result of crustal thickening and accretionary complex from the subduction. The Bitlis–Pötürge massif displays high velocities along the collision zone and uniform lower velocities on the Arabian platform.

A more quantitative analysis will be presented in the future by the joint inversion of group velocities with receiver functions and *Pn* velocities. Additional observations from ambient noise correlations may improve tomographic images in the areas with low ray coverage. Rayleigh wave observations with earthquakes and ambient noise correlations are in progress and will provide better resolution and higher sensitivity on the deeper part of the crust and mantle.

ACKNOWLEDGMENTS

We would like to thank Michel Pasyanos, an anonymous reviewer and the Associate Editor, Saskia Goes for their critical reviews, Helle A. Pedersen for providing the RMFA code for group velocity measurements. We also would like to thank Esen Arpat and Serdar Özalaybey for reading the manuscript and suggestions. Some of the figures were generated using the Generic Mapping Tools (GMT) software (Wessel & Smith 1998).

REFERENCES

Aki, K. & Richards, P.G., 1980. *Quantitative Seismology, Theory and Methods,* Vol. 2, W.H. Freeman and company, NY.

Aksu, A.E., Calon, T.J., Hall, J., Mansfield, S. & Yasar, D., 2005. The Cilicia–Adana basin complex, Eastern Mediterranean: Neogene evolution of an active fore-arc basin in an obliquely convergent margin, *Mar. Geol.,* **221,** 121–159.

Akyol, N., Zhu, L., Mitchell, B.J., Sözbilir, H. & Kekovalı K., 2006. Crustal structure and local seismicity in Western Anatolia, *Geophys. J. Int.,* **166/3,** 1259–1269.

Al-Lazki, A., Şeber, D., Sandvol, E., Turkelli, N., Mohamad, R. & Barazangi, M., 2003. Tomographic Pn velocity and anisotropy structure beneath the Anatolian Plateau (Eastern Turkey) and the surrounding regions, *Geophys. Res. Lett.,* **30**(24), doi:10.1029/2003GL017391.

Aydın, I., Karat, H.I. & Kocak, A., 2005. Curie-point depth map of Turkey, *Geophys. J. Int.,* **162,** 633–640.

Curtis, A., Trampert, J., Snieder, R. & Dost, B., 1998. Eurasian fundamental mode surface wave phase velocities and their relationship with tectonic structures, *J. geophys. Res.,* **103,** 26 919–26 947.

DiLuccio, F. & Pasyanos, M.E., 2007. Crustal and upper-mantle structure in the eastern Mediterranean from the analysis of surface wave dispersion curves, *Geophys. J. Int.,* **169,** 1139–1152.

Dziewonski, A.M., Bloch, S. & Landisman, M., 1969. A technique for the analysis of transient seismic signals, *Bull. seism. Soc. Am.,* **59**(1), 427–444.

Dziewonski, A.M., 1971. On regional differences in dispersion of mantle waves, *Geophys. J. R. astr. Soc.,* **22,** 289–325.

Engdahl, E.R., Van Der Hilst, R. & Buland, R., 1998. Global teleseismic earthquake relocation with improved travel times and procedures for depth determination. *Bull. seism. Soc. Am.,* **88,** 722–743.

Floyd, P.A., Göncüoglu, M.C., Winchester, J.A. & Yalınız, M.K., 2000. Geochemical character and tectonic environment of Neotethyan Ophiolitic fragments and metabasites in the Central Anatolian Crystalline Complex, Turkey, in *Tectonic and Magmatism in Turkey and the Surrounding Area,* Vol. 173, pp. 183–202, eds Bozkurt, E., Winchester, J.A. & Piper, J.D.A., Geological Society, Special Publications, London.

Glover, C. & Robertson, A.H.F., 1998. Neogen intersection of the Aegean and Cyprus arcs: extensional and strike-slip faulting in the Isparta Angle, SW Turkey. *Tectonophysics,* **298,** 103–132.

Göncüoğlu, M.C., Dürük, K. & Kozlu, H., 1997. General characteristics of pre-Alpine and Alpine Terranes in Turkey: explanatory notes to the terrane map of Turkey, *Annales Geologique de Pays Hellenique,* **37,** 515–536.

Gök, R., Sandvol, E., Turkeli, N., Seber, D. & Barazangi, M.M., 2003. Sn attenuation in the Anatolian and Iranian plateaus and surrounding regions, *Geophys. Res. Lett.,* **30**(24), 8042, doi:10.1029/2003GL018020.

Gök, R., Pasyanos, M.E. & Zor, E., 2007. Lithospheric structure of the continent–continent collision zone: eastern Turkey, *Geophys. J. Int.,* **169,** 1079–1088.

Herrmann, R.B., 2002. *Computer Programs in Seismology, Version 3.30,* St. Louis University, Missouri.

Innocenti, F., Manetti, P., Mazzuoli, R., Pasquaré G. & Villari, L., 1982. Anatolia and North-Western Iran, in *Andesites: Orogenic Andesites and*

Related Rocks, pp. 327–349, ed. Thorpe, R.S., TheOpen Univ., Dept. Earth Sci., Milton Keynes, UK.

Karagianni, E.E. *et al*., 2002. Rayleigh wave group velocity tomography in the Aegean area, *Tectonophysics,* **358,** 187–209.

Karagianni, E.E., Papazachos, C.B., Panagiotopoulos, D.G., Suhadolc, P., Vuan, A. & Panza, G.F., 2005. Shear velocity structure in the Aegean area obtained by inversion of Rayleigh waves, *Geophys. J. Int.,* **160,** 127–143.

Keskin, M., 2003. Magma generation by slab steepening and breakoff beneath a subduction–accretion complex: an alternative model for collision-related volcanism in Eastern Anatolia, Turkey, *Geophys. Res. Lett.,* **30,** 8046.

Knopoff, L., 1972. Observation and inversion of surface wave dispersion, *Tectonophysics,* **13,** 497–519.

Laigle, M., Becel, A., De Voogd, B., Hirn, A., Taymaz, T. & Özalaybey, S., 2008. A first deep seismic survey in the Sea of Marmara: deep basins and whole crust architecture and evolution, *Earth planet. Sci. Lett.,* **270**(3–4), 168–179.

Levshin, A.L., Ratnikova, L.I. & Berger, J., 1992. Peculiarities of surface wave propagation across central Eurasia, *Bull. seism. Soc. Am.,* **82,** 2464–2493.

Levshin, A.L., Ritzwoller, M.H. & Ratnikova, L.I., 1994. The nature and cause of polarization anomalies of surface waves crossing northern and central Eurasia, *Geophys. J. Int.,* **117,** 577–590.

Levshin, A.L., Barmin, M.P., Ritzwoller, M.H. & Trampert, J., 2005. Minor-arc and major-arc global surface wave diffraction tomography, *Phys. Earth planet. Inter.,* **149,** 205–223.

Maggi A. & Priestly, K., 2005. Surface waveform tomography of the Turkish–Iranian plateau, *Geophys. J. Int.,* **160,** 1068–1080.

Mindevalli, O.Y. & Mitchell, M.J., 1989. Crustal structure and possible anisotropy in Turkey from seismic surface wave dispersion, *Geophys. J. Int.,* **98,** 93–106.

Mooney, W., Laske, G. & Master, T., 1998. CRUST 5.1: a global crustal model at 5 × 5, *J. geophys. Res.* **103,** 727–747.

Nikishin, A.M., Korotaev, M.V., Ershov, A.V. & Brunet, M-F., 2003. The Black Sea basin: tectonic history and Neogene–Quaternary rapid subsidence modeling, *Sediment. Geol.,* **156,** 149–168.

Okay, A.I., 1989. Tectonic units and sutures in the Pontides, northern Turkey, in *Tectonic Evolution of the Tethyan Region,* pp. 109–115, ed. Şengör, A.M.C., Kluwer Academic Publications, Dordrecht.

Okay, A.I., Şengör, A.M.C. & Görür, N., 1994. Kinematic history of the opening of the Black Sea and its effect on the surrounding regions. *Geology,* **22,** 267–270.

Okay, A.I. & Tüysüz, O., 1999. Tethyan sutures of northern Turkey, in *"The Mediterranean Basins: Tertiary Extension within the Alpine orogen",* pp. 475–515, eds Durand, B., Jolivet, L., Horváth, F. & Séranne, M., Geological Society, Special Publication 156, London.

Oliver, J., 1962. A summary of observed surface wave dispersion, *Bull. seism. Soc. Am.,* **52,** 81–86.

Pasyanos, M., 2005. A variable resolution surface wave dispersion study of Eurasia, North Africa, and surrounding regions, *J. geophys. Res.,* **149,** 462–480.

Pasyanos, M., Walter, W. & Hazler, S., 2001. A surface wave dispersion study, of the Middle East and North Africa for monitoring the comprehensive nuclear test ban treaty, *Pure appl. Geophys.,* **158,** 1445–1474.

Pedersen, H.A., Mars, J.I. & Amblard, P.O., 2003. Improving surface wave group velocity measurements by energy reassignment, *Geophysics,* **68,** 679–684.

Ritzwoller, M.H. & Levshin, A.L., 1998. Eurasian surface wave tomography: group velocities, *J. geophys. Res.,* **103,** 4839–4878.

Ritzwoller, M.H., Shapiro, N.M., Barmin, M.P. & Levshin, A.L., 2002. Global surface wave diffraction tomography, *J. geophys. Res.,* **107,** 2335, doi:10.1029/2002JB001777.

Robertson, A.H.F., 2000. Mesozoic-Tertiary tectonic-sedimentary evolution of a South Tethyan oceanic basin and its margin in Southern Turkey, in *Tectonics and Magmatism in Turkey and the Surrounding Area,* Vol. 173, pp. 97–138, eds Bozkurt, E., Winchester, J.A. & Piper, J.D.A., Geological Society, Special Publications, London.

Robinson, A.G. (Ed.), 1997. *Regional and Petroleum Geology of the Black Sea and Surrounding Region*, Vol. 68, 385 pp. American Association of Petroleum Geologists, Memoir, Tulsa, OK, USA.

Sandvol, E., Turkelli, N. & Barazangi, M., 2003. The Eastern Turkey Seismic Experiment: the study of a young continent—continent collision, *Geophys. Res. Lett.,* **30**(24), 8038, doi:10.1029/2003GL018912.

Saunders, P., Priestly, K. & Taymaz, T., 1998. Variations in the crustal structure beneath Western Turkey, *Geophys. J. Int.,* **134,** 373–389.

Seymen, İ., 1984. Geological evolution of the metamorphic rocks of the Kırşehir Massif (in Turkish). in *Proceedings of the Ketin Symposium,* pp. 133–148 , Geological Society, Ankara, Turkey.

Sodoudi, F. *et al.,* 2006. Lithospheric structure of the Aegean obtained from P and S receiver functions, *J. geophys. Res.,* **111,** B12307, doi:10.1029/2005JB003932.

Spadini, G., Robinson, A. & Cloetingh, S., 1996. Western versus Eastern Black Sea tectonic evolution: pre-rift lithospheric controls on basin formation, *Tectonophysics,* **266,** 139–154.

Stampfli, G.M., 2000. Tethyan Oceans, in *Tectonic and Magmatism in Turkey and the Surrounding Area,* Vol. 173, eds Bozkurt, E., Winchester, J.A. & Piper, J.D.A., pp. 1–23, Geological Society, Special Publications, London.

Şengör, A.M.C. & Yılmaz, Y., 1981. Tethyan evolution of Turkey, a plate tectonic approach, *Tectonophysics,* **75,** 181–241.

Şengör, A.M.C., Yılmaz, Y. & Ketin, İ., 1982. Remnants of a pre-Late Jurassic ocean in northern Turkey, Fragments of Permo-Triassic Paleo-Tethys ?: reply, *Geol. Soc. Am. Bull.,* **93,** 932–936.

Şengör, A.M.C., Özeren, S., Genc, T. & Zor, E., 2003. East Anatolian high plateau as a mantle-supported, N–S shortened domal structure, *Geophys. Res. Lett.,* **30,** 8044, doi:10.1029/2003GL017858.

Tatar O., Piper J.D. & Gürsoy, H., 2000, "Paleomagnetic study of the Erciyes sector of the Ecemiş Fault Zone: neotectonic deformation in the southeastern part of the anatolian Block," in *Tectonics and Magmatism in Turkey and the Surrounding Area,* Vol. 173, pp. 423–440, eds Bozkurt, E., Winchester, J.A. & Piper, J.D.A., Geological Society, Special Publications, London.

Trampert, J. & Woodhouse, J.H., 1995. Global phase velocity maps of Love and Rayleigh waves between 40 and 150 seconds, *Geophys. J. Int.,* **122,** 675–690.

Tsai, Y. & Aki, B.K., 1971. Amplitude spectra of surface waves from small earthquakes and underground nuclear explosions, *J. geophys. Res.,* **76,** 3940–3952.

Toprak, V. & Göncüoğlu, M.C., 1993. Tectonic control on the development of the Neogene–Quaternary Central Anatolian volcanic province, *Turkey. Geol. J.,* **28,** 357–369.

Topuz, G., Altherr, R., Kalt, A., Satır, M., Werner, O. & Schwardz, W.H., 2004. Aluminus granulites from the Pulur complex, NE Turkey: a case of partial melting, efficient melt extraction and crystallization, *Lithos,* **72,** 183–207.

van Heijst, H.J. & Woodhouse, J., 1999. Global high-resolution phase velocity distributions of overtone and fundamental-mode surface waves determined by mode branch stripping, *Geophys. J. Int.,* **137,** 601–620.

Vdovin, O., Rial, J.A., Levshin, A.L. & Ritzwoller, M.H., 1999. Group velocity tomography of South America and the surrounding oceans, *Geophys. J. Int.,* **136,** 324– 340.

Wessel, P. & Smith, W.H.F., 1998. New, improved version of Generic Mapping Tools released, *EOS, Trans. Am. geophys. Un.,* **79,** 579.

Woodhouse, J.H. & Dziewonski, A.M., 1984. Mapping the upper mantle: three-dimensional modeling of earth structure by inversion of seismic wavefroms, *J. geophys. Res.,* **89,** 5953–5986.

Yılmaz, Y., 1993. New evidence and model on the evolution of the southeast Anatolian orogen, *Geol. Soc. Am. Bull.,* **105,** 251–271.

Yılmaz, Y., Guner Y. & Saroglu, F., 1998. Geology of the Quaternary volcanic centers of the east Anatolia, *J. Volc. Geotherm. Res.,* **85,** 173–210.

Zhu, L., Mitchell, B.J., Akyol, N., Cemen, I. & Kekovali, K., 2006. Crustal thickness variations in the Aegean region and implications for the extension of continental crust, *J. geophys. Res.,* **111,** B01301. doi:10.1029/2005JB003770.

Zor, E., Sandvol, E., Gürbüz, C., Turkeli, N., Şeber, D. & Barazangi, M., 2003. The crustal structure of the East Anatolian Plateau (Turkey) from receiver functions, *Geophys. Res. Lett.,* **30**(24), 8044, doi:10.1029/2003GL018192.

Zor, E., Özalaybey, S. & Gürbüz, C., 2006. The crustal structure of the Eastern Marmara Region (Turkey) by teleseismic receiver functions, *Geophys. J. Int.,* **167,** 213–222.

SUPPORTING INFORMATION

Additional Supporting Information may be found in the online version of this article:

Figure S1. Examples of waveforms recorded at various distances (red) and reassigned multiple-filter analysis with picked dispersion values (blue marks).

Please note: Wiley-Blackwell are not responsible for the content or functionality of any supporting materials supplied by the authors. Any queries (other than missing material) should be directed to the corresponding author for the article.

© 2010 The Authors, *GJI*, **181,** 502–520
Journal compilation © 2010 RAS